

Cite this: *Chem. Sci.*, 2019, **10**, 7059 All publication charges for this article have been paid for by the Royal Society of ChemistryReceived 1st May 2019  
Accepted 11th June 2019DOI: 10.1039/c9sc02127b  
[rsc.li/chemical-science](http://rsc.li/chemical-science)

## Stereochemical significance of O to N atom interchanges within cationic helicenes: experimental and computational evidence of near racemization to remarkable enantiospecificity†

Geraldine M. Labrador, <sup>a</sup> Céline Besnard, <sup>b</sup> Thomas Bürgi, <sup>c</sup> Amalia I. Poblador-Bahamonde, <sup>\*a</sup> Johann Bosson <sup>\*a</sup> and Jérôme Lacour <sup>\*a</sup>

Oxygen atoms of cationic dioxa and azaoxa [6]helicenes can be exchanged by amino groups to form azaoxa and diaza [6]helicenes respectively. The mild reaction conditions developed herein allow the construction of libraries of derivatives with sensitive and/or functionalized side chains. Using enantioenriched dioxa or azaoxa helicene precursors, these exchanges lead to either near racemization (es 3%) or to a remarkable enantiospecificity (es up to 97%). This unusual behavior is fully characterized via experimental and computational mechanistic evidence. Based on these investigations, the enantiospecificity of the first transformation can be improved to 57–61%.

## Introduction

Pioneered by Baeyer and Piccard more than a century ago,<sup>1–3</sup> the formation of pyridinium ions by treatment of pyrylium salts with primary amines is recognized as a method of choice for the construction of cationic aza aromatics (Fig. 1, top).<sup>4–6</sup> The three step reaction mechanism, *i.e.*, (i) the nucleophilic attack of the amine, (ii) the O-ring opening yielding an intermediate ketone and (iii) the N-ring closure on the carbonyl,<sup>7–10</sup> classes this reaction as an ANRORC process.<sup>11</sup> The driving force of the transformation is the better stabilization of the positive charge by the more electron-donating amino group. When the pyrylium unit is embedded in a polycyclic scaffold, the reaction suffers from a breaking of the overall aromaticity upon O-ring opening. The transformation of xanthylium salts to acridinium ions is thus more challenging but it remains possible as exemplified by the groups of Laursen, Müllen or recently Nicewicz, usually in moderate yields.<sup>12–16</sup> The amenability of this transformation to non-planar chiral polycyclic systems, and helicenes in particular, was questionable. In fact, with strained substrates like helicenes, the occurrence of more stable (sterically less-demanding) ring-opened biaryl intermediates might disfavor the final ring closure. Conversely, extension of this strategy to cationic oxa helicenes would allow

the rapid construction of libraries of aza helicenes,<sup>17–19</sup> compounds that are attractive in regard of their applications in chemistry and at the interface of biology and physics.<sup>20–25</sup> This methodology would also be an interesting addition to the field of late-stage functionalization that remains challenging in polycyclic aromatics.<sup>26–33</sup> Finally, enantiospecific substitutions of O by N atoms within the helicene outer rim would be a novelty in the helicene field. Herein the pyrylium to pyridinium route is extended to cationic [6]helicenes,<sup>34,35</sup> and the direct transformation of dioxa **1** into azaoxa **2** and ultimately into diaza **3** is demonstrated (Fig. 1, bottom). The reaction conditions are sufficiently mild to introduce tailored and/or chemically sensitive functional groups (24 examples). From **2** to **3**, the reaction is enantiospecific (es up to 97%, retention of configuration), which is in stark contrast to the conversion of **1** into **2** for which an almost racemization occurs (es 3%). In-depth experimental and computational investigations of the reaction profiles reveal, in this latter case, the occurrence of propeller intermediates that can racemize through a series of two ring flip processes.<sup>36</sup> After adaptation of the experimental conditions to limit such deleterious pathways, reaction **1** to **2** then occurs with an effective transfer of the stereochemical information (es 57–61%).

## Results and discussion

In the initial report,<sup>34</sup> hetero helicenes **1**, **2** and **3** were prepared using a common acyclic triarylcyclopropane precursor and then three different ring closing routes, each at very high temperatures (>170 °C, Schemes S1 and S2†). The synthesis of dioxa **1** was particularly efficient as it was obtained in 95% yield in

<sup>a</sup>Department of Organic Chemistry, University of Geneva, Switzerland. E-mail: Amalia.PobladorBahamonde@unige.ch; johann.bosson@unige.ch; jerome.lacour@unige.ch

<sup>b</sup>Laboratory of Crystallography, University of Geneva, Switzerland

<sup>c</sup>Department of Physical Chemistry, University of Geneva, Switzerland

† Electronic supplementary information (ESI) available. CCDC 1908256 and 1908257. For ESI and crystallographic data in CIF or other electronic format see DOI: 10.1039/c9sc02127b



## Pyrylium to pyridinium salts via ring openings / closures

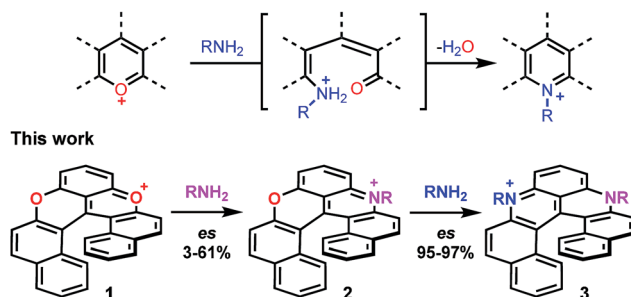


Fig. 1 Top: conversion of pyrylium to pyridinium ions via sequences of ring openings and ring closures. Bottom: enantiospecific transformations of cationic dioxo and mono oxa [6]helicenes to the corresponding aza derivatives.

5 min in molten Pyr·HCl. For the construction of aza helicenes 2 and 3, it was only possible to introduce amines with linear alkyl chains in low to moderate yields; amines substituted with (sensitive) functional groups were incompatible. In this context, the possibility to use dioxo 1 as a unique precursor to prepare derivatives 2 and 3 in one step *via* a “pyrylium to pyridinium” strategy was deemed not only interesting but also advantageous considering the ready availability of 1 in large scale and high yield by the previous method. This was put to the test. Experimentally the addition of an excess of *n*-propyl amine (25 equiv.) to a solution of dioxo 1 in NMP resulted in an immediate color change from red to blue. Upon heating at 70 °C for 7 h, the formation of diaza 3a was evidenced (ESI-MS monitoring, 13% isolated yield). After this result, reaction conditions were optimized (Tables S1–S3†). A reduction of the amount of amine (3 equiv.) and the use of benzoic acid as additive (1.5 equiv.) afforded the preferential formation of azaoxa 2a in 3 h at 60 °C in 38% yield.<sup>37</sup> Upon increasing the reagents’ stoichiometry (25 equiv. of amine and 12.5 equiv. of benzoic acid) along with a prolonged reaction time (7 h) at 70 °C, dioxo 1 was converted into diaza 3a in 47% yield. The same reaction conditions also afforded diaza 3a from azaoxa 2a in 36% yield (Fig. 1, R = *n*-propyl).

With the mild conditions developed above, the scope of the reaction was extended. The preparation of azaoxa derivatives 2b to 2i was investigated (Fig. 2). A focus was given to the introduction of residues which were not tolerated before. For instance, *n*-octyl 2b was obtained in 26% yield. More sterically demanding *i*-propyl amine yielded 2c (20% yield). Redox sensitive benzyl and allyl amines were readily introduced (compounds 2d and 2e, 20% and 23% respectively).<sup>15,38,39</sup> Alcohol, carboxylic acid and ester functional groups were also compatible with the reaction conditions (compounds 2f–2h, 29%, 29% and 25% respectively). Finally, PEG functionalized azaoxa helicene 2i was obtained in 25% yield.

Next, the preparation of symmetrical diaza [6]helicenes 3b to 3i using dioxo 1 as substrate was studied (Fig. 3). Introduction of linear alkyl or alcohol chains proceeded unsurprisingly as 3b or 3f were isolated in moderate yields (24 and 26%, respectively). As for compound 2c, it was possible to introduce an

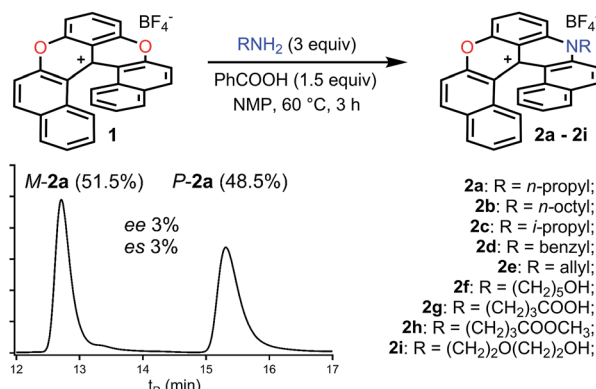


Fig. 2 Transformation of dioxo 1 into azaoxa 2a to 2i. Inset: CSP HPLC trace of 2a (enantiospecificity es 3% starting from (−)-M-1, ee 98%).

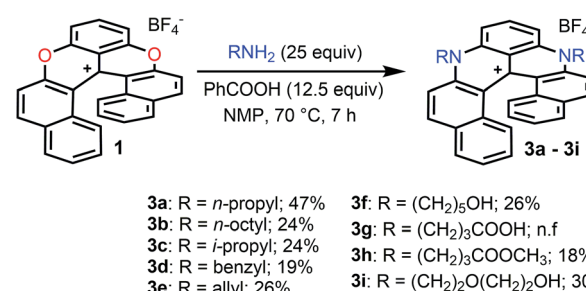


Fig. 3 Transformation of dioxo 1 into diaza 3a to 3i. n.f.: not formed.

isopropyl residue (3c, 24% yield). Interestingly, diaza [6]helicenes 3d and 3e with dibenzyl and diallyl side chains were also accessible (19% and 26%). While, to our surprise, a simple carboxylic acid moiety could not be added (3g), the methyl ester analogue was integrated to the helical scaffold (3h, 18%). Bis PEGylated helicene 3i was also isolated in 30% yield.

Finally, compounds 2 were also transformed into diaza 3 giving access to unsymmetrically substituted analogues 3j to 3p (Fig. 4). For instance, *n*-propyl azaoxa helicene 2a was easily converted into diaza helicenes 3j (12%), 3k (38%) and 3l (17%) by reactions with aliphatic *n*-octyl, sterically hindered *i*-propyl and allyl amines respectively. Hydroxyl functionalized diaza helicenes 3m and 3n were also readily prepared from 2a (26% and 19% yield respectively). PEG functionalized azaoxa 2i was converted into diaza helicene 3o bearing an isopropyl group (23%) while substrate 2d led to the formation of diaza 3p bearing both sensitive benzyl and hydroxypentyl moieties (25%).

Importantly, reactions 1 → 2a, 1 → 3a and 2a → 3a were then performed with enantioenriched substrates to determine, as mentioned earlier, if the substitution(s) of the O by N atoms could occur enantiospecifically. This was in fact debatable as the S<sub>N</sub>(ANRORC) mechanism offers *a priori* many possibilities for a loss of enantiomeric purity after ring opening steps in particular. Practically, *rac*-1, *rac*-2a and *rac*-3a were resolved by chiral stationary phase (CSP) HPLC into the corresponding *M*



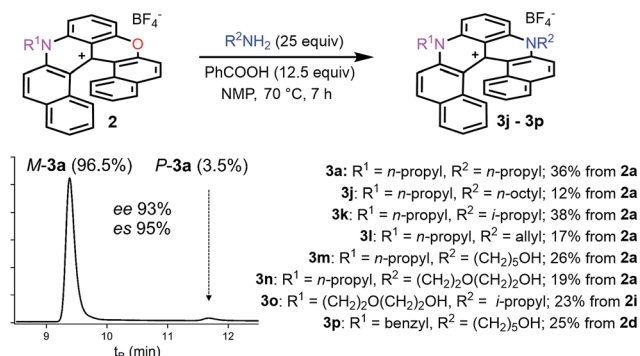


Fig. 4 Transformation of azaoxa 2 into diaza 3. Inset: CSP HPLC trace of  $3\text{a}$  (ee 95% starting from  $(-)\text{-}M\text{-}2\text{a}$ , ee 98%).

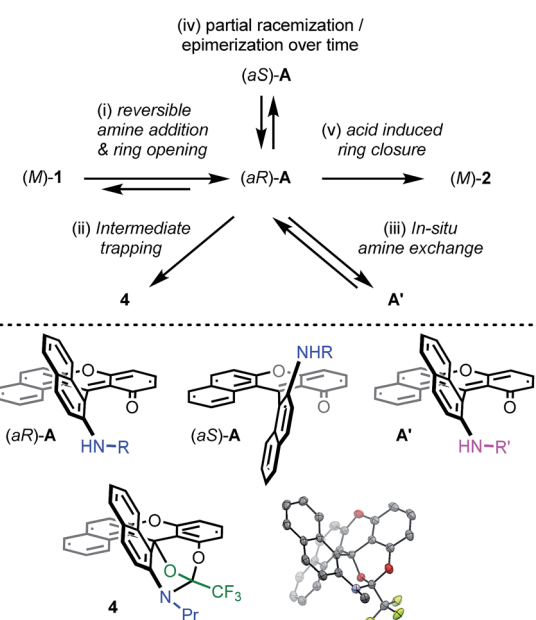


Fig. 5 Top: summary of mechanistic investigations. (i)  $\text{RNH}_2$  (3 equiv.),  $20^\circ\text{C}$ ,  $\text{CH}_3\text{CN}$ ; then work-up with water to establish the reversibility. (ii)  $\text{F}_3\text{CCOCl}$  (12 equiv.),  $\text{CH}_3\text{CN}$ ,  $20^\circ\text{C}$ , 16 h, 4 (57%). (iii) Evaporation then  $\text{R}'\text{NH}_2$  (3 equiv.),  $20^\circ\text{C}$ ,  $\text{CH}_3\text{CN}$ . (iv) Addition of (*S*)-methyl-*tert*-butylamine and  $^1\text{H}$  NMR monitoring (see Fig. 6). (v) Evaporation then benzoic acid (1.5 equiv.), NMP,  $60^\circ\text{C}$ , 3 h. Bottom: chemical structures of intermediates  $(aR)\text{-A}$ ,  $(aS)\text{-A}$  and  $A'$ . Drawing and ORTEP view of the crystal structure of 4: hydrogen atoms are omitted and the propyl chain is truncated for clarity reasons.

and *P* enantiomers (ee 97–99%). Compounds **1**, **2a** and **3a** are configurationally stable at elevated temperatures, up to 110, 150 and  $>180^\circ\text{C}$  specifically.<sup>34,40</sup> The absolute configuration of the enantiomers of **1** and **2a** was unknown prior to this study. It was established by vibrational circular dichroism (VCD) thanks to the conformational rigidity of the compounds that helped the determination (see ESI, Fig. S18–S23†). Interestingly, in this series which also includes **3a**,<sup>40</sup> the dextro and levorotatory enantiomers are of *P* and *M* configurations irrespectively of their dioxa, azaoxa or diaza nature.

Then, attempts to prepare **2a** starting from enantiopure (+) and (−)-**1** led unfortunately to the formation of (+)-*P*- and (−)-*M*-**2a** in only marginal enantiomeric excesses (ee 3%). Similarly, **3a** was obtained from enantiopure (+)- and (−)-**1** in almost racemic form (4% and 0% ee for the (+)- and (−)-enantiomers respectively). In striking contrast, conversion of azaoxa (+)-*P*- and (−)-*M*-**2a** (ee 99 and 98%) provided diaza (+)-*P*- and (−)-*M*-**3a** in 96 and 93% ee, indicating this time a very high level of enantiospecificity for the O to N exchange (ee 97–95%). The three transformations detailed above, and **2a**  $\rightarrow$  **3a** in particular, occur hence with retention of configuration.<sup>41</sup> With these results in hand, experimental and theoretical investigations were performed to determine the mechanism. The aim was to understand the reactivity pathways including their stereochemistry, measure the importance of additives like benzoic acid or offer prospects on how to limit the racemization. Various intermediates, products of trapping experiments and reaction processes were identified. They are summarized in Fig. 5 and specific details are given in the following paragraphs.

## Mechanistic evidence

First, dioxa helicene **1** was treated at ambient temperature with an excess of  $^n\text{PrNH}_2$  which led to one intermediate, named **A**, almost instantly and quantitatively. In the absence of benzoic acid and in the given reaction time (3 h), the reaction did not proceed further. To our surprise, any attempt to isolate this intermediate after aqueous workup led to the complete recovery of starting dioxa **1**. The reaction  $\mathbf{1} \rightleftharpoons \mathbf{A}$  is thus fully reversible in the presence of water.<sup>42</sup> Detailed *in situ* NMR spectroscopy and MS analyses revealed that **A** possesses a biaryl structure with the N atom connected to the naphthyl ring as a result of a regioselective O-ring opening (see ESI, Fig. S1†). The structure of **A** was indirectly confirmed by the isolation and X-ray structural analysis of *leuco* compound **4** (see ESI and CCDC 1908256†); this derivative results from the addition of an excess of trifluoroacetyl chloride to **A** (Fig. 5). Also, if a different amine is added to **A**, then full substitution of the first amine by the second is evidenced in  $^1\text{H}$  NMR spectroscopy. This exchange forming intermediate **A'** shows (again) the reversibility of amine additions as observed experimentally by the replacement of  $^n\text{Pr}$  by  $^n\text{Pr}$  residues ( $\mathbf{A} \rightleftharpoons \mathbf{A}'$ , Fig. S2 and S3†).

Of particular interest for the stereochemistry of the process, (*S*)-methyl-*tert*-butylamine was added to enantiopure (−)-*M*-dioxa [6]helicene **1**. Upon addition, a single set of NMR signals was observed for intermediate **A** (Fig. 6, spectrum (a), see also Fig. S4 in the ESI†). For instance, signals of protons  $\text{H}_7$  and  $\text{H}_9$  appeared as simple doublets at 6.23 and 5.98 ppm respectively. However, after 3 h at  $60^\circ\text{C}$  (Fig. 6, spectrum (b)), all the mentioned doublets, and some other signals, were split in two. The crude, which was composed initially of a single species (spectrum (a)) has now become a mixture of two stereoisomers in a 88 : 12 ratio.<sup>43</sup> Importantly, spectrum (b) is similar and opposite to spectrum (c) that is obtained upon the reaction of (*S*)-methyl-*tert*-butylamine with (+)-*P*-**1**. In this latter case, the

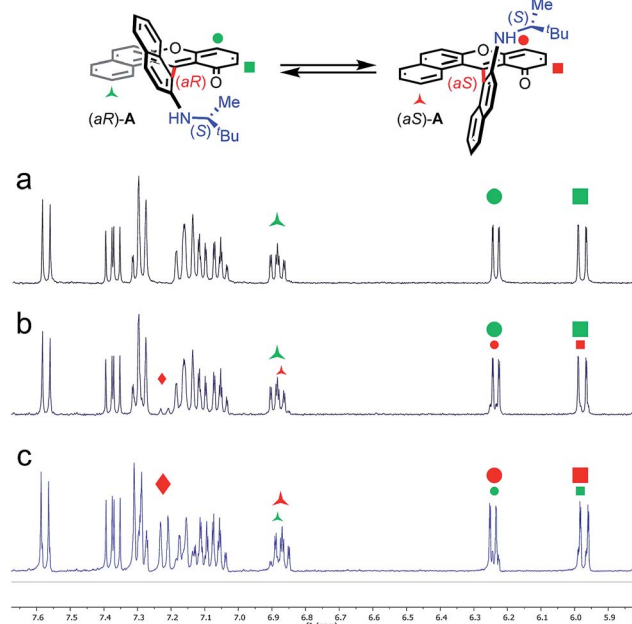


Fig. 6 Diastereoisomers of **A** prepared with (S)-methyl-tert-butylamine.  $^1\text{H}$  NMR spectroscopy performed at 400 MHz in  $\text{CD}_3\text{CN}$ . Spectrum (a):  $(-)\text{-M-1}$  with excess (S)-methyl-tert-butylamine after 5 min at  $20\text{ }^\circ\text{C}$ , d.r.  $> 49 : 1$ . Spectrum (b):  $(-)\text{-M-1}$  with excess (S)-methyl-tert-butylamine after 3 h at  $60\text{ }^\circ\text{C}$ , d.r.  $88 : 12$ . Spectrum (c):  $(+)\text{-P-1}$  with excess (S)-methyl-tert-butylamine after 3 h at  $60\text{ }^\circ\text{C}$ , d.r.  $21 : 79$ .  $\blacktriangle = \text{H}_2$ ,  $\bullet = \text{H}_7$ ,  $\blacksquare = \text{H}_9$ ,  $\blacklozenge = \text{not attributed}$ .

presence of two diastereoisomers also occurs after some time at  $60\text{ }^\circ\text{C}$ . The diastereomeric ratio of  $88 : 12$  (spectrum (b)) is now inverted to a  $21 : 79$  value (spectrum (c), see also Fig. S5 in the ESI $\dagger$ ). Clearly, in the span of the reaction, an epimerization/racemization process occurs at the stage of intermediate **A** but only to a minimal extent; some further steps must happen to account for the almost complete racemization observed at the end of the process. In Fig. 6 are represented the geometry of the stereoisomers of **A** obtained upon addition of the chiral amine onto  $(-)\text{-M-1}$ ; the configuration of the epimers was determined in the course of the study (*vide infra*).

Finally, it was established that **A** is a productive intermediate as, in the presence of benzoic acid (1.5 equiv.) at  $60\text{ }^\circ\text{C}$  (3 h), **A** transforms itself into the corresponding helicene **2a**. The presence of the carboxylic acid is essential for the way forward and its role in the promotion of the aza ring closure will be clearly demonstrated by the theoretical analysis (*vide infra*). Conversely the use of sodium benzoate alone provided **2a** in only 4% yield (see Table S3 $\dagger$ ). Other acids like  $^7\text{PrNH}_3\text{Cl}$  (3 equiv.) did not induce the formation of the azaoxa [6]helicene.

In conclusion for this section, experimental evidence was found to shed some light on the mechanism of the transformation of **1** to **2a**, and on the existence of intermediates of type **A** or **A'**. Structural and energetical aspects of the process were however hard to apprehend. Care was thus taken to perform an extensive computational survey of the reaction pathway which is depicted in Fig. 7 starting from  $(M)\text{-1}$  (energy profile).<sup>44</sup>

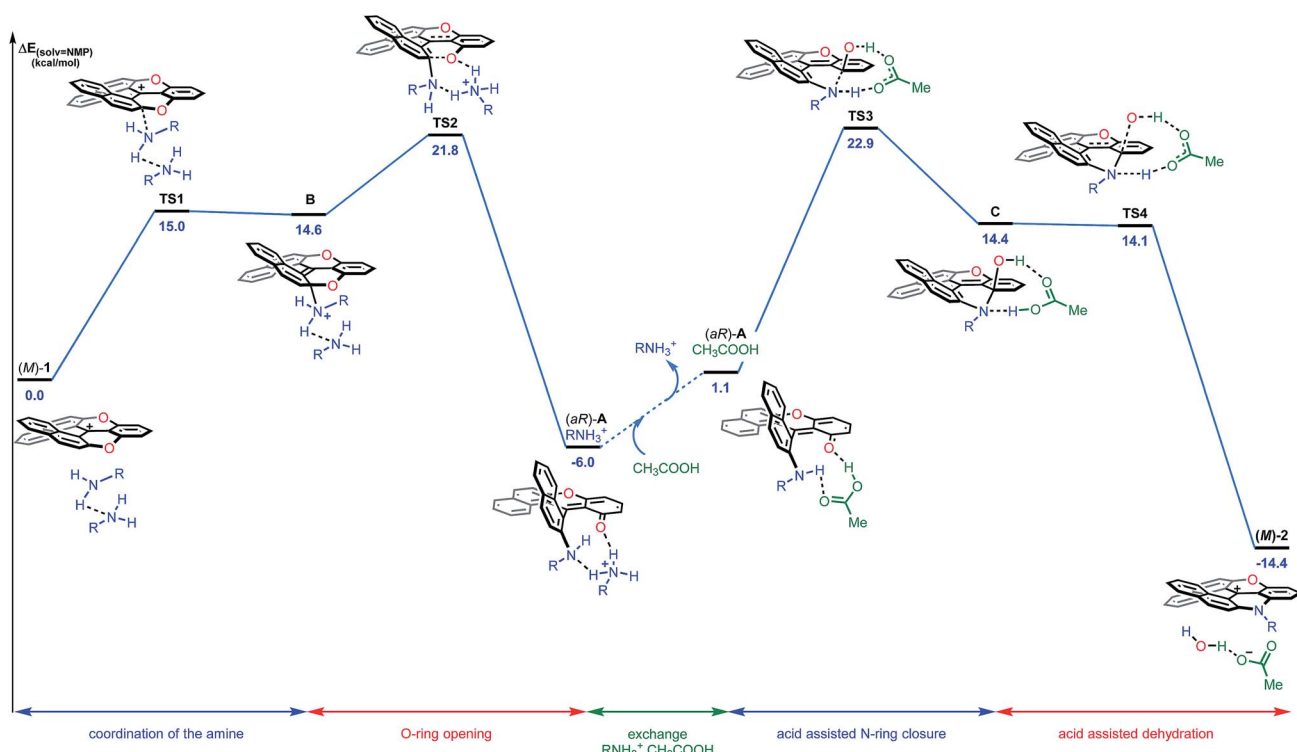


Fig. 7 Reaction energy profile of the transformation of  $(-)\text{-(}M\text{)-dioxia 1 into }(-)\text{-(}M\text{)-azaoxa 2}$  ( $\text{R} = \text{methyl}$ ). The reported PCM energies (solvent = NMP) are given in  $\text{kcal mol}^{-1}$ .



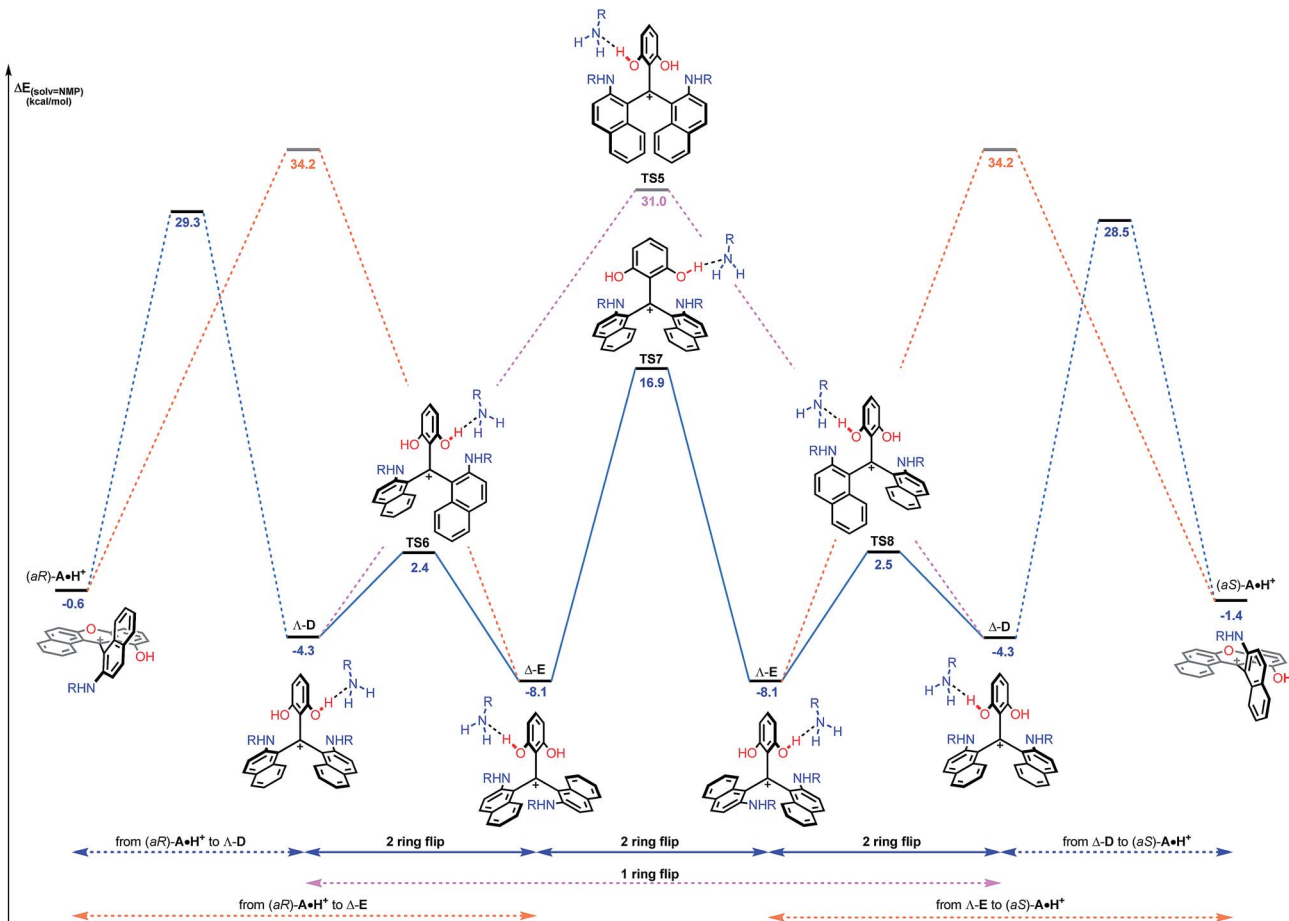


Fig. 8 Reaction energy profile of the enantiomerization from  $(aR)$ -A·H<sup>+</sup> to  $(aS)$ -A·H<sup>+</sup>. The ring opening of  $(aR)$ -A·H<sup>+</sup> from the *Re* face leading to  $\Delta$ -D (blue dashed lines) and from the *Si* face leading to  $\Delta$ -E (orange dashed lines) are detailed in the ESI.† Direct isomerization of  $\Delta$ -D into  $\Delta$ -D (pink dashed lines) is clearly not favored. The reported PCM energies (solvent = NMP, R = methyl) are given in kcal mol<sup>-1</sup>.

## Theoretical study

Computationally, the experimental excess of amine (3 equiv.) was modelled using a bis-amine cluster. The nucleophilic attack, which occurs exclusively on the naphthyl subunits, can happen on the *Re* and *Si* faces of **1**, and both approaches were simulated. The reaction that occurs on the *Re* face of (*M*)-dioxia **1** proceeds through a late transition state **TS1** ( $\Delta E^\ddagger = +15.0$  kcal mol<sup>-1</sup>) which models the dearomatization of the naphthyl moiety and leads to the unstable ammonium adduct **B** ( $\Delta E = +14.6$  kcal mol<sup>-1</sup>). The following carbon oxygen bond cleavage occurs *via* a 6-membered transition state **TS2** at 21.8 kcal mol<sup>-1</sup> and it generates stabilized intermediate  $(aR)$ -**A** that possesses an *ortho* quino methide character ( $\Delta E = -6.0$  kcal mol<sup>-1</sup>).<sup>45</sup> Importantly, a strong association with the bis-amine cluster occurs and the positive charge is now localized on the H-bonded ammonium adduct. The attack on the *Si* face follows a similar behavior although in this case, intermediate **A** is highly distorted and clearly unfavorable energetically ( $\Delta E(\mathbf{A}_{Re}) = -6.0$  kcal mol<sup>-1</sup> vs.  $\Delta E(\mathbf{A}_{Si}) = +5.7$  kcal mol<sup>-1</sup>, Fig. S24†). These observations are in adequacy with the experimental results and the existence of a highly stereospecific

formation of **A**, at the beginning of the reaction in particular. It is rooted in the facial *Re* selectivity of the O-ring opening of dioxia (*M*)-**1** and, hence, in the stereocontrolled formation of biaryl  $(aR)$ -**A**.

For the subsequent conversion of intermediate **A** to azaoxa **2**, an explicit carboxylic acid molecule is required computationally to reproduce well the experimental observations. Calculations show that the replacement of the ammonium ion by the carboxylic acid destabilizes the supramolecular adduct, from  $-6.0$  to  $1.1$  kcal mol<sup>-1</sup>. Once the acid coordinated, the desired N-ring closure happens *via* **TS3** ( $\Delta E^\ddagger = +22.9$  kcal mol<sup>-1</sup>) and forms **C**. During the C–N bond formation, the carboxylic acid acts as a proton shuttle helping the approach of the nucleophile by promoting simultaneously the deprotonation of the amino group and the protonation of the oxygen atom. Then, dehydration of **C** occurs in a barrier-less process and provides azaoxa (*M*)-**2** that is more stable than the starting dioxia (*M*)-**1** by 14.4 kcal mol<sup>-1</sup>.<sup>46</sup> Overall, the transformation from the ammonium adduct  $(aR)$ -A·H<sub>3</sub>NR to **C** constitutes the rate determining step ( $\Delta E^\ddagger = +28.9$  kcal mol<sup>-1</sup>). An analogous computational study was performed starting from (*P*)-**1** and leading to the formation of (*P*)-**2**; throughout the study, an

opposite *as* configuration for intermediate **A** was evidenced (see ESI, Fig. S25†).

While this theoretical approach (Fig. 7) accounted well for the reactivity profile of the reaction, the above calculations did not rationalize the isolation of **2** in almost racemic form starting from either (*M*)-**1** or (*P*)-**1**. In fact, as detailed above, the O-ring opening of dioxa (*M*) or (*P*)-**1** is enantiospecific and leads to intermediates (*aR*) and (*as*)-**A** which in turn are converted to azaoxa (*M*) and (*P*)-**2** respectively. Also, as shown in the experiments with (*S*)-methyl-*tert*-butylamine (Fig. 6), intermediates of type **A** are quite configurationally stable in basic medium at 60 °C. The origin of the racemization was thus debatable and the possibility of an equilibrium between intermediates (*aR*)-**A** and (*as*)-**A** induced by an acidification was considered (Fig. 8). As a matter of fact, upon protonation, (*aR*)-**A** is transformed into (*aR*)-**A**·H<sup>+</sup> in which the positive charge is localized on the xanthenium core. This species is highly electrophilic and, as a consequence, it reacts further with the excess of amine cleaving the second ether linkage. Again, this attack can formally occur from either *Re* and *Si* faces of (*aR*)-**A**·H<sup>+</sup> leading to the formation of two three-bladed propellers, named **Δ-D** and **Δ-E**; the  $\Delta$  and  $\Lambda$  prefixes corresponding to the left and right handed propeller configurations respectively as the additions behave stereoselectively. In **D**, the two amino groups point inward, *i.e.* toward the central phenyl ring while in **E**, one amino group is directed toward the center and the other outward. The global energy profiles, depicted in Fig. 8, clearly indicate the preferential kinetic formation of **Δ-D** over **Δ-E** (see the ESI for more details, Fig. S26 and S27†).<sup>47</sup> However, the enantiomerization of **Δ-D** into **Δ-D**, through **TS5**, is highly disfavored ( $\Delta E = +35.3$  kcal mol<sup>-1</sup>) and follows an unusual one ring flip route in which the transition state deviates from ideality; the distortion is brought by the steric hindrance of the naphthyl units.<sup>36,48</sup> Alternatively, stepwise isomerization of **Δ-D** into **Δ-D** was computed through a first facile isomerization of **Δ-D** into **Δ-E** that follows a two ring flip mechanism, *via* **TS6** ( $\Delta E^\ddagger = +6.7$  kcal mol<sup>-1</sup>), in which one of the larger naphthyl group remains in the main plane. Subsequent enantiomerization from **Δ-E** to **Δ-E**, also modeled through a two ring flip mechanism with **TS7** located at +16.9 kcal mol<sup>-1</sup>, then accounts for the racemization observed under acid conditions. In fact, (*as*)-**A**·H<sup>+</sup> is readily obtained *via* the antipodal route from **Δ-E** and **Δ-D** leading to a globally facile (*aR*)-**A**  $\rightleftharpoons$  (*as*)-**A** equilibrium under acidic conditions.<sup>49</sup> Noteworthy, the isomerizations of **Δ-D** into **Δ-D** and of **Δ-E** into **Δ-E** were also computed in the absence of the extra H-bonded amine; quite higher energies for the associated TS were obtained in both cases (see ESI, Fig. S28–S30†).<sup>50</sup> It is also worth to mention that propeller intermediates **D** and **E** were detected by *in situ* mass spectrometry and their presence explain as well the formation of dibenzoacridinium **5** which can be isolated as a side product (10–30% yield, Fig. 9).<sup>51</sup> In fact, a relatively simple pathway was computed for its formation from **Δ-E** *via* intermediate **F** and an acid-promoted cyclization/deamination (Fig. 9); the overall kinetic barrier is compatible with the experimental observation of **5** ( $\Delta E^\ddagger = +17.5$  kcal mol<sup>-1</sup>).

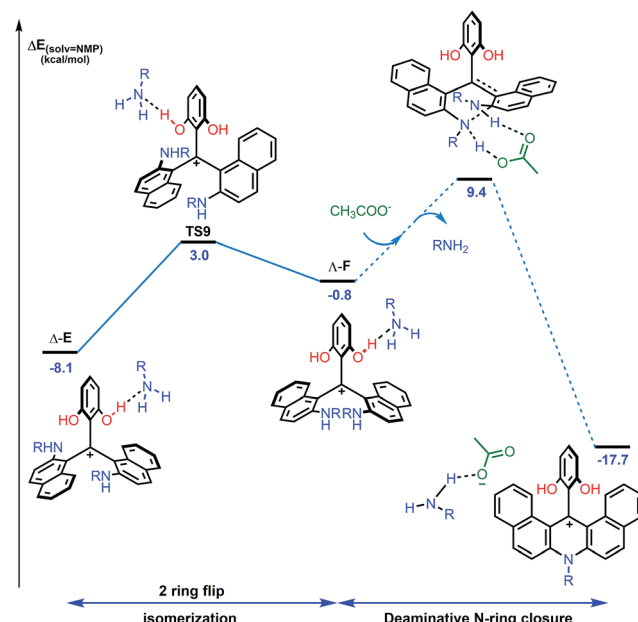


Fig. 9 Reaction energy profile for the isomerization from  $\Delta$ -E to  $\Delta$ -F and subsequent formation of dibenzoacridinium **5** *via* an acid-promoted cyclization/deamination sequence. The details of the pathway from  $\Delta$ -F to **5** (dashed lines) are depicted in the ESI, Fig. S33.† The reported PCM energies (solvent = NMP, R = methyl) are given in kcal mol<sup>-1</sup>.

## Toward higher level of enantiospecificity

According to the mechanistic scheme detailed above (Fig. 8), the racemization observed during the formation of azaoxa **2** occurs *via* three-bladed propeller intermediates of type **D** and **E** that necessitates both an acid activation and an excess of primary amine to cleave all ether linkages. To overcome this deleterious effect, it was decided to employ a strict stoichiometric amount of primary amine (for the O to N ring exchange) along with an excess of non-nucleophilic Hunig's base to buffer the medium. Furthermore, to avoid the build-up of species **A** (responsible for the racemization), a slow addition of this combination of nucleophilic and non-nucleophilic amines was considered. With this set of conditions (Fig. 10), the enantiospecificity of the transformation from **1** to **2a** was in part recovered (es 61% and 57% with (*M*)-**1** and (*P*)-**1** respectively, Fig. S12 and S13†). The reactions occurred with retention of the configuration as it could be expected from the computational study. Unfortunately, the yield of (*M*) or (*P*)-**2a** was drastically lowered to 6% only.

In addition, as mentioned earlier, conversion of (+)-*P*- and (−)-*M*-**2a** provides diaza (+)-*P*- and (−)-*M*-**3a** with very high enantiospecificity (es 97–95%) for the O to N exchange. Computationally, the reaction proceeds in a similar fashion to that from **1** to **2**. Ring opening of *M*-**2** with an excess of primary amine leads to the formation of intermediate (*aR*)-**G** located at −4.4 kcal mol<sup>-1</sup> (Fig. 11a and S34† for details).<sup>52</sup> This ring opening is regioselective (Fig. S8†) and it was evidenced experimentally by the trapping of **G** with 4-chlorobenzoyl

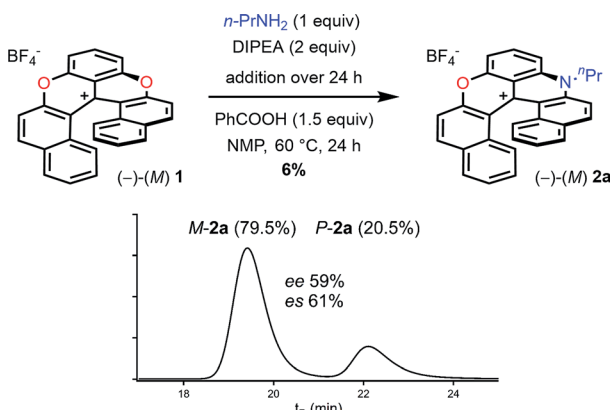


Fig. 10 Transformation of dioxo  $(-)$ -M-1 into azaoxa  $(-)$ -M-2a. Inset: CSP HPLC trace of 2a (enantiospecificity es 61% starting from  $(-)$ -M-1, ee 97%).

chloride to afford 6 (63%, Fig. 11b and CCDC 1908257<sup>†</sup>). This step is clearly stereoselective as evidenced by <sup>1</sup>H-NMR monitoring upon addition of (*S*)-methyl-*tert*-butylamine acting as stereochemical probe. As detailed in Fig. S9,<sup>†</sup> the NMR spectrum of the addition adduct displays signals for a single stereoisomer which is stable at 70 °C for 7 h. Not surprisingly, the subsequent aza ring closure from (*aR*)-G to M-3 (located at  $-16.6$  kcal mol<sup>-1</sup>) is also facilitated by the presence of benzoic acid that promotes the proton transfer and the final dehydration. Yet, the 2  $\rightarrow$  3 transformation differs from 1  $\rightarrow$  2 in two aspects. First, the O-ring opening is rate determining this time

(TS10  $+27.9$  kcal mol<sup>-1</sup>). Second, and of utmost importance for the enantiospecificity, protonated intermediate  $\mathbf{G}\cdot\mathbf{H}^+$  does not react with an excess of primary amine (Fig. 11c). Both *Re* and *Si* face approaches and subsequent reactivities would proceed with very high activation energies ( $+48.6$  and  $+54.3$  kcal mol<sup>-1</sup>, respectively) and would be thermodynamically disfavored with corresponding propeller adducts located at  $+43.1$  and  $+40.5$  kcal mol<sup>-1</sup> (see ESI, Fig. S36 and S37<sup>†</sup>). This explains the large stereochemical difference between reactions 1  $\rightarrow$  2 and 2  $\rightarrow$  3 – something that was hard to predict at the onset of the project.

## Conclusions

Herein the transformation of pyrylium rings into pyridinium cycles has been extended to the field of cationic helicenes. The replacement of oxygen atom(s) at the outer rim by stabilizing amino groups proceeds *via* S<sub>N</sub>Ar mechanisms. The reported reaction conditions are sufficiently mild to be beneficial for the introduction of functional groups that were not tolerated previously (24 examples). In-depth mechanistic studies, experimental and theoretical, demonstrate that the process is enantiospecific (es up to 97% for 2  $\rightarrow$  3) and occurs with retention of configuration. Near racemization can however happen *via* three-bladed propeller intermediates, if starting from dioxo 1 in particular. Based on the mechanistic understanding, corrective measures were applied to recover a large amount of the enantiospecificity for the 1  $\rightarrow$  2 process (es 57–61%). Care will be taken to utilize this late-stage functionalization strategy for future developments and applications of these original chromophores and fluorophores.<sup>53–61</sup>

## Conflicts of interest

There are no conflicts to declare.

## Acknowledgements

Initial CSP-HPLC resolutions of the helicenes were performed by the team of Dr Eric Francotte (Novartis, Basel) in the framework of a previous study.<sup>40</sup> We thank the University of Geneva, the DIP-State of Geneva and the Swiss National Science for funding and support. We also acknowledge the contributions of the Sciences Mass Spectrometry (SMS) platform at the Faculty of Sciences, University of Geneva. The contribution of Stéphane Grass and Marion Pupier for HPLC and NMR analyses are appreciated. We also thank Carmine Chiancone for technical support.

## Notes and references

- 1 A. Baeyer, *Ber. Dtsch. Chem. Ges.*, 1910, **43**, 2337–2343.
- 2 A. Baeyer and J. Piccard, *Justus Liebigs Ann. Chem.*, 1911, **384**, 208–224.
- 3 D. A. Conlon, in *Name Reactions in Heterocyclic Chemistry II*, John Wiley & Sons, Inc., 2011, ch. 6.1, pp. 338–346.

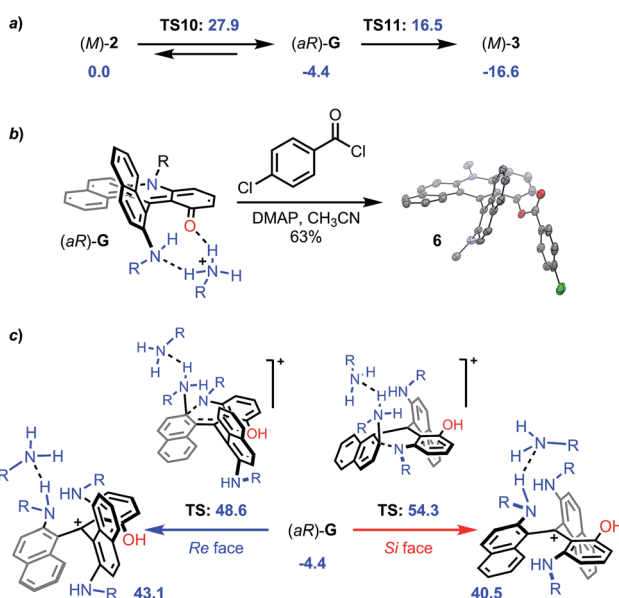


Fig. 11 The reported PCM energies (R = methyl, solvent = NMP) are given in kcal mol<sup>-1</sup>. (a) Energies of the general transformation from (M)-2 to (M)-3 via intermediate (aR)-G. (b) Trapping of intermediate G yielding 6; ORTEP view of the crystal structure of 6; hydrogen atoms are omitted and the propyl chains are truncated for clarity reasons. (c) Energies of the N-ring openings of (aR)-G from the *Re* and the *Si* faces. DMAP = 4-N,N-dimethylaminopyridine.



4 R. J. Aarons, K. Afarinkia, A. T. Balaban, T. S. Balaban, N. Camp, S. Faulkner, P. J. Murphy, A. Nelson, M. Nográdi, W.-D. Rudorf, V. Vinader, R. C. Whitehead and A. C. Williams, in *Category 2, Hetarenes and Related Ring Systems*, ed. E. J. Thomas, Georg Thieme Verlag, Stuttgart, 2003 edn, 2003, vol. 14.1, pp. 11–200.

5 S. Sowmia, J. M. S. S. Esperanca, L. P. N. Rebelo and C. A. M. Afonso, *Org. Chem. Front.*, 2018, **5**, 453–493.

6 For recent applications, see: M. Wang, K. Wang, C. Wang, M. Huang, X.-Q. Hao, M.-Z. Shen, G.-Q. Shi, Z. Zhang, B. Song, A. Cisneros, M.-P. Song, B. Xu and X. Li, *J. Am. Chem. Soc.*, 2016, **138**, 9258–9268; D. Moser, Y. Duan, F. Wang, Y. Ma, M. J. O'Neill and J. Cornella, *Angew. Chem., Int. Ed.*, 2018, **57**, 11035–11039; F. J. R. Klauck, H. Yoon, M. J. James, M. Lautens and F. Glorius, *ACS Catal.*, 2019, **9**, 236–241.

7 A. T. Balaban and C. Toma, *Tetrahedron*, 1966, **22**, 1–8.

8 A. R. Katritzky and R. H. Manzo, *J. Chem. Soc., Perkin Trans. 2*, 1981, 571–575.

9 A. R. Katritzky, J. M. Lloyd and R. C. Patel, *J. Chem. Soc., Perkin Trans. 1*, 1982, 117–123.

10 A. R. Katritzky, R. H. Manzo, J. M. Lloyd and R. C. Patel, *Angew. Chem., Int. Ed.*, 1980, **19**, 306.

11 H. C. Van der Plas, *Acc. Chem. Res.*, 1978, **11**, 462–468.

12 M. Rosenberg, K. R. Rostgaard, Z. Liao, A. Ø. Madsen, K. L. Martinez, T. Vosch and B. W. Laursen, *Chem. Sci.*, 2018, **9**, 3122–3130.

13 I. Bora, S. A. Bogh, M. Rosenberg, M. Santella, T. J. Soerensen and B. W. Laursen, *Org. Biomol. Chem.*, 2016, **14**, 1091–1101.

14 D. Wu, X. Feng, M. Takase, M. C. Haberecht and K. Müllen, *Tetrahedron*, 2008, **64**, 11379–11386.

15 B. W. Laursen and F. C. Krebs, *Chem.-Eur. J.*, 2001, **7**, 1773–1783.

16 A. R. White, L. Wang and D. A. Nicewicz, *Synlett*, 2019, **30**, 827–832.

17 F. Dumitrescu, D. G. Dumitrescu and I. Aaron, *ARKIVOC*, 2010, 1–32.

18 L. Adriaenssens, L. Severa, T. Šálová, I. Císařová, R. Pohl, D. Šaman, S. V. Rocha, N. S. Finney, L. Pospíšil, P. Slavíček and F. Teplý, *Chem.-Eur. J.*, 2009, **15**, 1072–1076.

19 S. Arai, T. Yafune, M. Ōkubo and M. Hida, *Tetrahedron Lett.*, 1989, **30**, 7217–7218.

20 I. G. Stara and I. Stary, *Sci. Synth.*, 2010, **45b**, 885–953.

21 Y. Shen and C.-F. Chen, *Chem. Rev.*, 2011, **112**, 1463–1535.

22 M. Gingras, *Chem. Soc. Rev.*, 2013, **42**, 1051–1095.

23 J. Bosson, J. Gouin and J. Lacour, *Chem. Soc. Rev.*, 2014, **43**, 2824–2840.

24 N. Hoffmann, *J. Photochem. Photobiol., C*, 2014, **19**, 1–19.

25 C.-F. Chen and Y. Shen, *Helicene Chemistry: From Synthesis to Applications*, Springer, Berlin, Heidelberg, 2017.

26 D. Schweinfurth, M. Mazzolini, D. Neshchadin, C. Hoyer, R. Geier, K. Gatterer, N. Trapp, G. Gescheidt and F. Diederich, *Chem.-Eur. J.*, 2016, **22**, 7152–7157.

27 I. H. Delgado, S. Pascal, A. Wallabregue, R. Duwald, C. Besnard, L. Guenée, C. Nancoz, E. Vauthey, R. C. Tovar, J. L. Lunkley, G. Muller and J. Lacour, *Chem. Sci.*, 2016, **7**, 4685–4693.

28 M. Hasan, A. D. Pandey, V. N. Khose, N. A. Mirgane and A. V. Karnik, *Eur. J. Org. Chem.*, 2015, **2015**, 3702–3712.

29 A. Bucinskas, D. Waghray, G. Bagdziunas, J. Thomas, J. V. Grazulevicius and W. Dehaen, *J. Org. Chem.*, 2015, **80**, 2521–2528.

30 M. Weimar, R. Correia da Costa, F.-H. Lee and M. J. Fuchter, *Org. Lett.*, 2013, **15**, 1706–1709.

31 S. K. Surampudi, G. Nagarjuna, D. Okamoto, P. D. Chaudhuri and D. Venkataraman, *J. Org. Chem.*, 2012, **77**, 2074–2079.

32 A. Rajca, M. Pink, S. Xiao, M. Miyasaka, S. Rajca, K. Das and K. Plessel, *J. Org. Chem.*, 2009, **74**, 7504–7513.

33 A. A. Ruch, S. Handa, F. Kong, V. N. Nesterov, D. R. Pahls, T. R. Cundari and L. M. Slaughter, *Org. Biomol. Chem.*, 2016, **14**, 8123–8140.

34 F. Torricelli, J. Bosson, C. Besnard, M. Chekini, T. Bürgi and J. Lacour, *Angew. Chem., Int. Ed.*, 2013, **52**, 1796–1800.

35 J. Bosson, G. M. Labrador, S. Pascal, F.-A. Miannay, O. Yushchenko, H. Li, L. Bouffier, N. Sojic, R. C. Tovar, G. Muller, D. Jacquemin, A. D. Laurent, B. Le Guennic, E. Vauthey and J. Lacour, *Chem.-Eur. J.*, 2016, **22**, 18394–18403.

36 K. Mislow, *Acc. Chem. Res.*, 1976, **9**, 26–33.

37 The beneficial role of benzoic acid in  $S_NAr$  reactions has been already observed by Laursen and co-workers. See for instance ref. 12.

38 C. Nicolas, C. Herse and J. Lacour, *Tetrahedron Lett.*, 2005, **46**, 4605–4608.

39 B. Laleu, C. Herse, B. W. Laursen, G. Bernardinelli and J. Lacour, *J. Org. Chem.*, 2003, **68**, 6304–6308.

40 G. M. Labrador, J. Bosson, Z. S. Breitbach, Y. Lim, E. R. Francotte, R. Sabia, C. Villani, D. W. Armstrong and J. Lacour, *Chirality*, 2016, **28**, 282–289.

41 Later in the manuscript, it will be shown that the transformation of  $(+)$ -1a  $\rightarrow$   $(+)$ -2a and of  $(-)$ -1a  $\rightarrow$   $(-)$ -2a can occur with an improved enantiospecificity of 57–61%; this result establishes firmly the retention of configuration upon heteroatom exchange.

42 It will be later shown that the observation of A is driven by the formation of an ammonium adduct ( $\Delta E = -6.0$  kcal mol $^{-1}$ ). Removal of the ammonium interaction destabilizes the structure by at least +12.6 kcal mol $^{-1}$  and this explains the reversibility upon hydrolysis.

43 A related experiment was performed in ECD ( $\text{CH}_3\text{CN}$ ,  $2 \times 10^{-5}$  M) upon the addition of *n*-propylamine onto enantiopure  $(+)$ -1. While an immediate transformation of the ECD spectrum was noticed upon the formation of A, the Cotton effects did not evolve over time upon heating at 50 °C for 1 h 30. This indicates that the nature of the amine probably influences the kinetics of epimerization of A and that less-sterically demanding amines such  $\text{PrNH}_2$  might favor enantiospecific pathways. See the ESI, Fig. S6 and S7.†

44 For examples of DFT calculations on related compounds, see for instance: S. Lemke, S. Ulrich, F. Claussen, A. Bloedorn, U. Jung, R. Herges and O. M. Magnussen, *Surf. Sci.*, 2015, **632**, 71–76; H. Jacob, S. Ulrich, U. Jung, S. Lemke,



T. Rusch, C. Schütt, F. Petersen, T. Strunkus, O. Magnussen, R. Herges and F. Tuczek, *Phys. Chem. Chem. Phys.*, 2014, **16**, 22643–22650.

45 E. E. Kwan, Y. Zeng, H. A. Besser and E. N. Jacobsen, *Nat. Chem.*, 2018, **10**, 917–923.

46 For examples of chirality transfer from biaryl species to ring closed helicenes, see M. Murai, R. Okada, A. Nishiyama and K. Takai, *Org. Lett.*, 2016, **18**, 4380–4383; K. Nakano, Y. Hidehira, K. Takahashi, T. Hiyama and K. Nozaki, *Angew. Chem., Int. Ed.*, 2005, **44**, 7136–7138.

47 After the coordination of the amine, the O-ring opening requires a high activation energy of  $+29.3$  kcal mol $^{-1}$ . In addition, the formation of  $\Delta$ -D is thermodynamically favored starting from (aR)-A·H $^+$  ( $\Delta E = -4.3$  kcal mol $^{-1}$ ).

48 Traditionally, the enantiomerization of Ar<sub>3</sub>Z propellers containing two identical rings with local  $C_1$ -symmetry and one  $C_2$ -symmetrical ring occurs preferentially through two ring flip processes. See D. Gust and K. Mislow, *J. Am. Chem. Soc.*, 1973, **95**, 1535–1547.

49 The reaction pathway from (aS)-A·H $^+$  to dioxo **1** of (*P*) configuration is detailed in the ESI.†

50 H. Ito, T. Abe and K. Saigo, *Angew. Chem., Int. Ed.*, 2011, **50**, 7144–7147.

51 For the formation of related molecules *via* a pyrylium into pyridinium transformation, see ref. 14.

52 For the transformation from **2** to **3**, the energy of **2** is set at 0.0 kcal mol $^{-1}$ .

53 H. Isla and J. Crassous, *C. R. Chim.*, 2016, **19**, 39–49.

54 N. Saleh, C. Shen and J. Crassous, *Chem. Sci.*, 2014, **5**, 3680–3694.

55 P. Aillard, A. Voituriez and A. Marinetti, *Dalton Trans.*, 2014, **43**, 15263–15278.

56 Z. Jarolímová, J. Bosson, G. M. Labrador, J. Lacour and E. Bakker, *Electroanalysis*, 2018, **30**, 650–657.

57 Z. Jarolímová, J. Bosson, G. M. Labrador, J. Lacour and E. Bakker, *Electroanalysis*, 2018, **30**, 1378–1385.

58 C. Bauer, R. Duwald, G. M. Labrador, S. Pascal, P. Moneva Lorente, J. Bosson, J. Lacour and J.-D. Rochaix, *Org. Biomol. Chem.*, 2018, **16**, 919–923.

59 H. Li, A. Wallabregue, C. Adam, G. M. Labrador, J. Bosson, L. Bouffier, J. Lacour and N. Sojic, *J. Phys. Chem. C*, 2017, **121**, 785–792.

60 H. Li, S. Voci, A. Wallabregue, C. Adam, G. M. Labrador, R. Duwald, I. Hernández Delgado, S. Pascal, J. Bosson, J. Lacour, L. Bouffier and N. Sojic, *ChemElectroChem*, 2017, **4**, 1750–1756.

61 R. Duwald, S. Pascal, J. Bosson, S. Grass, C. Besnard, T. Bürgi and J. Lacour, *Chem.-Eur. J.*, 2017, **23**, 13596–13601.

